Synthetic pores with sticky π-clamps†

Hiroyuki Tanaka, Guillaume Bollot, Jiri Mareda, Svetlana Litvinchuk, Duy-Hien Tran, Naomi Sakai and Stefan Matile*

Received 12th February 2007, Accepted 19th March 2007
First published as an Advance Article on the web 3rd April 2007
DOI: 10.1039/b702255g

In this report, we describe design, synthesis, evaluation and molecular dynamics simulations of synthetic multifunctional pores with π-acidic naphthalenediimide clamps. Experimental evidence is provided for the formation of unstable but inert, heterogeneous and acid-insensitive dynamic tetrameric pores that are sensitive to base and ionic strength. Blockage experiments reveal that the introduction of aromatic electron donor–acceptor interactions provides access to the selective recognition of π-basic intercalators within the pore. This breakthrough is important for the application of synthetic pores as multianalyte sensors.

Introduction

Bifunctional acyclic receptors, a.k.a. molecular clamps,[1] tweezers,[2] clips,[3,4] clefts[5] or jaws[6] have stimulated the creativity of chemists since decades.[1–12] Molecular clamps continue to attract scientific attention because they provide access to the acyclic version of the inclusion complexes formed by macrocyclic receptors such as cyclophanes, carcerands, cryptophanes, calixarenes or larger architectures like biological and synthetic α-helix bundles or β-barrels. Bidentate coordination within molecular tweezers[12] as well as bifunctional intercalation into molecular π-clamps[1–11] has been particularly productive. π-Clamping with Whitlock's pioneering caffeine tweezers was found early on to increase with tweezer rigidity, improving molecular recognition of benzoates and naphthoates by about two orders of magnitude.[2] The reversed π-clamping of caffeine with the black tea polyphenol theaflavin is a fine example for the quite frequently observed π-clamping in biology and medicine.[7]

Other highlights in the history of π-clamping include Zimmerman's application of rigid acridine and phenanthrene tweezers to affinity chromatography of nitrated polycyclic aromatic hydrocarbons[8] or Nolte's glycoluryl clips.[3] The more recent Klärner series of tetra-, tri-, and dimethylene-bridged naphthalene and anthracene tweezers and clips revealed, *inter alia*, a rich collection of intercalators, usefulness of charge transfer for effective π-clamping, and stunning template effects that perfectly imitate the pinching action of tweezers on the molecular level.[4] Colquhoun has introduced pyrene tweezers to π-clamp macrocyclic naphthalenediimide (NDI) dimers.[9] Contributions from aromatic donor–acceptor interactions to adhesive π-clamping have been found recently for pentafluorobenzene dimers.[10] π-Clamping with acylic (and cyclic)[13] porphyrin dimers has been studied by several groups with regard to the recognition of fullerenes,[7,13] nucleotides[5] or alkyl viologens.[11] The programmed assembly of π-clamps into stacked rosettes reveals the close relation between π-clamping and broad field of intercalation.[14] Ion-pair assisted π-clamping of nucleotides on one side of a synthetic β-sheet has been achieved with a diagonal tryptophan (W) tweezer with flanking lysines (K).[15,16] It was this breakthrough by Butterfield and Waters that identified π-clamping as ideal to expand molecular recognition within synthetic pores[1,17] beyond ion pairing.

Synthetic multifunctional pores such as **1** are rigid-rod β-barrels (Fig. 1).[17–21] These barrel-stave supramolecules are composed of rigid-rod staves and β-sheet hoops. During self-assembly from monomeric *p*-oligophenyls (see Scheme 1), the non-planar staves help to roll the planar β-sheets into the cylindrical oligomers. In the final barrel, the β-sheet hoops help to position functional groups at outer and inner pore surfaces to maximize interactions with the surrounding bilayer and molecules passing through the pore, respectively. So far, internal molecular recognition has focused exclusively on topologically precise ion pairing. This simple and sloppy recognition motif within synthetic pores was already sufficient to develop applications in catalysis and sensing.[17–21] Highlights include synthetic pores as general optical transducers of chemical reactions[18] or multicomponent sensing in complex matrixes[19] exemplified with sugar sensing in Coke.[20] Refined pore designs have been realized to probe the importance of guest inclusion and template effects as well as the depth of inclusion.[21]

The introduction of recognition motifs beyond ion pairing is of very high interest considering the possible practical applications of synthetic ion channels and pores (for selected reviews and selected highlights on the topic of synthetic ion channels and pores, please see ref. 22–32). π-Clamping within synthetic multifunctional pores was particularly attractive because characteristics such as the salt effects are orthogonal to ion pairing. NDIs, unique, abiotic, compact, organizable,[33–43] colorizable[42,43] and functionalizable[36–38,42,43] n-semiconductors[39,40] were selected for π-clamping within synthetic multifunctional pore **2**. With a quadrupole moment of +19 B (Buckinghams),[38] the π-acidity of NDIs exceeds that of hexafluorobenzene as well as the π-basicity of higher aromatics such as pyrene (−14 B).[38] This high π-acidity is ideal for both self-assembly as well as the formation of face-to-face aromatic electron donor–acceptor (AEDA) complexes.[33–36]

Department of Organic Chemistry, University of Geneva, Geneva, Switzerland. E-mail: stefan.matile@chiorg.unige.ch; Fax: +41 22 379 5123; Tel: +41 22 379 6523

† Electronic supplementary information (ESI) available: Experimental details. See DOI: 10.1039/b702255g

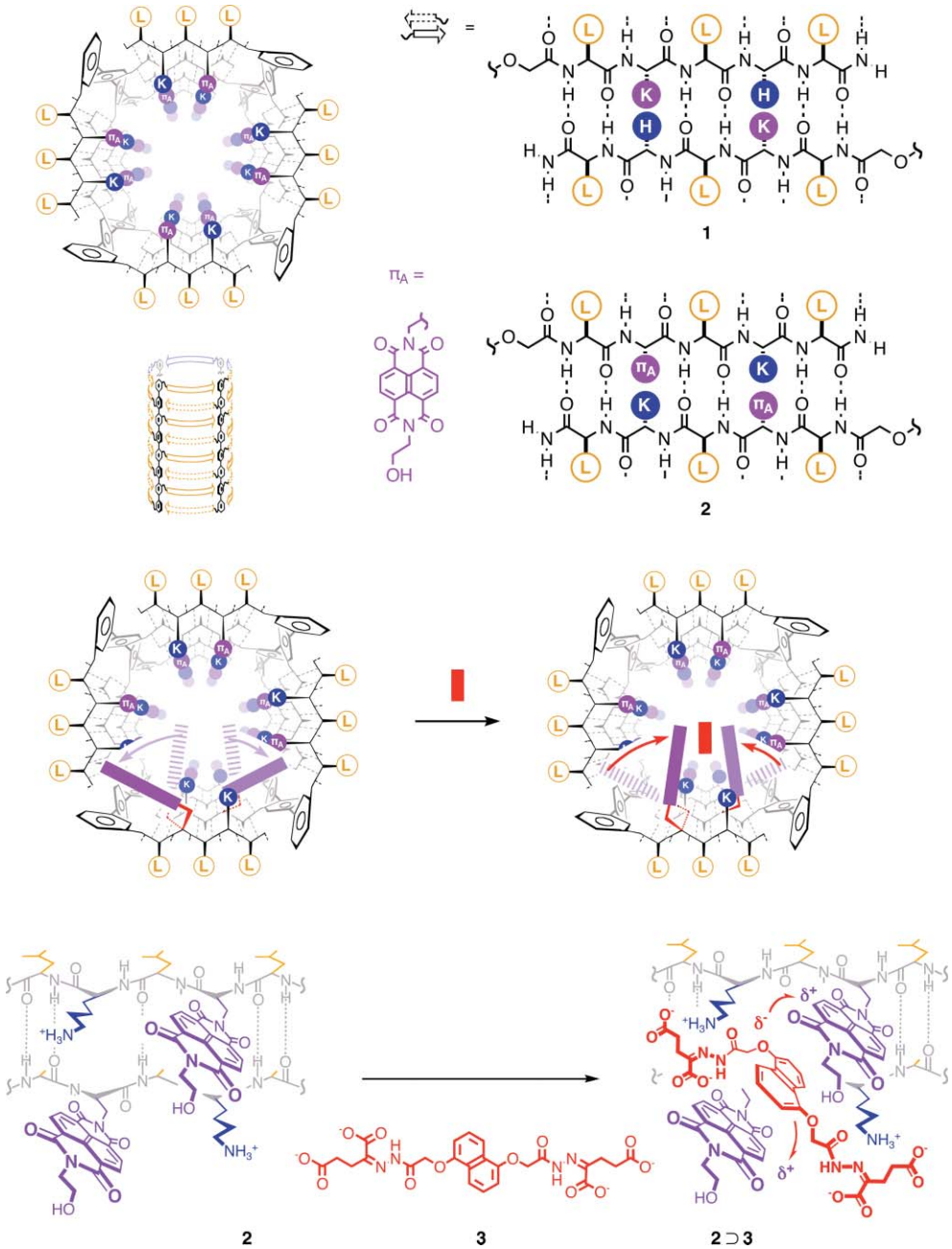

Fig. 1 Rigid-rod β-barrel pores **1** and **2** (top) with indication of possible π-clamp motions within the π-acidic pore **2** (arrows, middle) to catch the π-basic blocker **3** (red) in inclusion complex **2** ⊃ **3**, featuring the classical face-to-face DAN-NDI charge-transfer complex with operational aromatic electron donor–acceptor interactions (red half-arrows, bottom). β-Sheets are shown as solid (backbone) and dotted lines (hydrogen bonds, axial views) or as arrows (N → C, side view); external amino acid residues are dark on white, internal ones white on dark (single-letter abbreviations), see Fig. 2 and 3 for molecular models of pore **2** and pore-blocker complexes **2** ⊃ **3**, respectively.

Pioneered by Iverson with elegant foldamers,[33,34] AEDA complexes with the complementary dialkoxynaphthalenes (DANs) received particular attention for the creation of double helices,[34] barrel-stave supramolecules,[37,38] rotaxanes[35] or catenanes[35] that can act as shuttles,[35] stimuli-responsive gels,[36] ligand-gated ion channels[37] or anion-π slides.[38] NDI intercalation into π-stacks beyond DAN reaching from DNA duplexes[41] to pyrene tweezers[9] has been reported as well. The previous use of DAN-NDI interactions to open up helical rigid-rod π-stacks into small ion channels[37] can be considered as complementary to the present use to close large pores formed by rigid-rod β-barrels. The application of the underlying π-stack architecture for artificial photosynthesis[42,43] is conceptually complementary to the sensing applications of the β-barrel architecture used in this study.[18–20]

NDI clamps within synthetic pores were also of interest because they introduce rigid-rod β-barrels with artificial amino acids and are thus beyond reach or difficult to access with biological or bioengineered pores, respectively. Functional internal and external

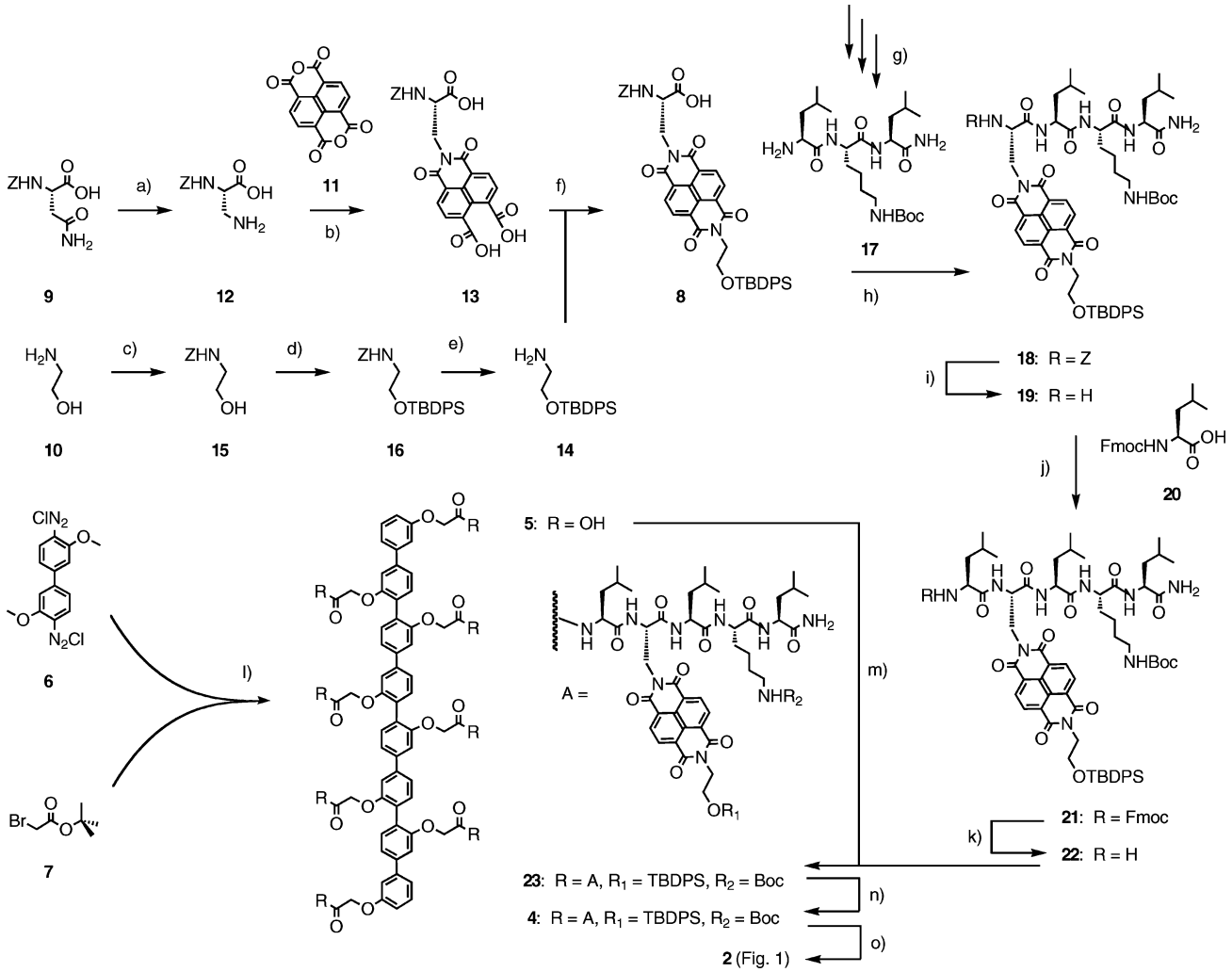

Scheme 1 Synthesis of multifunctional pore **2**. (a) $C_6H_5I(OAc)_2$, 92%.[67] (b) 1. NaOH, H_2O; 2. **12**, H_3PO_4, pH 5–7, 110 °C. (c) ZCl, Na_2CO_3, 48%. (d) TBDPSCl, imidazole, CH_2Cl_2, 0 °C, 1 h. (e) $Pd(OH)_2/C$, H_2, EtOH, quant.[68–70] (f) DMF, 110 °C; 70% from **12**. (g) 4 steps, see ref. 71 and 72. (h) HBTU, Et_3N, DMF, 84%. (i) $Pd(OH)_2/C$, H_2, DMF–MeOH (5 : 1), 80%. (j) HBTU, Et_3N, DMF, 70%. (k) 5% Piperidine–DMF, 64%. l) 9 steps, see ref. 63. (m) HATU, Et_3N, DMA, 99%. (n) 1. HF–Py, DMA, 2. TFA, 62%. (o) Self-assembly in lipid bilayer membranes.

rings of aromatics occur, however, quite frequently in biological and bioengineered pores. The aromatic rings at the pore exterior and at the membrane–water interface are unrelated to the topic of this study.[44–47] Internal aromatic rings, however, exist as well and play roles in protein translocation through and effective blockage (nanomolar IC_{50}s) of the Anthrax pore,[48] the blockage of potassium channels,[49] the selectivity of ammonia channels,[50] pH gating and blockage of the M2 channel from influenza-A virus with the antiviral amantadine (aminoadamantane),[51] and so on, often by cation–π interactions rather than π-clamping. Poor TNT recognition by aromatic rings engineered into the α-hemolysin pore (molar IC_{50}'s) illustrates that the introduction of aromatic rings into pores does not automatically result in effective π-clamping.[52]

In the following, we describe design, synthesis, evaluation and molecular dynamics simulations of synthetic multifunctional pores **2** with π-acidic NDI π-clamps. Experimental evidence is reported for the formation of unstable but relatively inert, heterogeneous and acid insensitive dynamic tetrameric pores that are sensitive to base, ionic strength and the selective recognition of nucleotides, π-basic naphthalenes and other intercalators by ion-pair assisted adhesive π-clamping (*e.g.*, **3**, Fig. 1). Selected highlights have been reported in the preliminary communication on the topic.[1]

Results and discussion

Design

Synthetic multifunctional pore **1** is one of the best explored rigid-rod β-barrel pores.[20,53,54] Leucines are placed at the outer surface as an ideal compromise between β-propensity and bilayer affinity.[17,44] Internal histidine-lysine (HK) dyads were introduced as binding sites for anionic molecules, thus allowing us to discriminate ATP and ADP with the "naked eye." This important function was of use to sense sugar in soft drinks with pore **1**.[20] Single-molecule images of pore-blocker complexes are also available.[54]

Synthetic multifunctional pore **2** was envisioned to expand molecular recognition beyond the dominant ion pairing in **1** and related rigid-rod β-barrel pores. For adhesive π-clamping, that is for molecular recognition by aromatic donor–acceptor interactions within pore **2**, pore **1** was changed as little as possible to assure maximal comparability. Histidine was replaced by the artificial NDI amino acid π_A (this arbitrary abbreviation was made to indicate a "π-acidic" amino-acid side chain, or a "π-acceptor"). The sequence of the internal residues was reversed to introduce the artificial NDI amino acid as late as possible in the pentapeptide synthesis. The ethanolamine as an NDI terminus was introduced to be able to solubilize intractable synthetic intermediates as bulky TBDPS derivatives (see below).

The assumption that the new pore **2** would be a tetramer was made based on extensive data available on this motif including pore **1**.[17–21] Namely, Hill plots for the self-assembly of the (unstable)[53,55] rigid-rod β-barrels with pentapeptide β-sheets including **1** have demonstrated self-assembly into tetramers. Hill plots of rigid-rod β-barrel **2** suggest that increasing internal crowding with the bulky NDIs is, in contrast to other examples,[56] insufficient to cause supramolecular barrel expansion into higher oligomers (see below).

Molecular dynamics simulations were compatible with tetrameric active structures (Fig. 2) as well as selective pore blockage by aromatic electron donor–acceptor interactions (Fig. 3). The structures shown were obtained following previously established protocols.[57] In brief, MacroModel version 7.0[58,59] coupled with a Maestro 4.1 graphical interface[60] was used first to assemble and preoptimize pore **2**. Close contacts were eliminated with the MMFF94s force field[61] and the Polak–Ribiere conjugate gradient (PRCG) algorithm. The empty barrel **2** was submitted to 2 ns MD simulations using AMBER 8.[62] Additional molecular dynamics of 2 ns were performed for barrels where the π-clamping with an aromatic electron donor was modeled. Such simulation times were adequate for equilibration of these systems in the gas phase.

In agreement with pH profiles (see below), lysine residues were fully protonated to assure the internal charge repulsion needed to stabilize internal space and prevent its collapse.[53,57] In the modeled pore, the bulky NDIs were found to preferably reside in loosely packed π-stacks located towards the pore walls and over the *p*-octiphenyl turns. Consistent with high activity (see below), this architecture yielded a wide-open pore. The minimal inner pore diameter was $d = 1.0$ nm. This diameter was in agreement with the observed efflux of CF (5(6)-carboxyfluorescein, minimal outer diameter = 1.0 nm) and the observed high conductance of single pores (see below). The *P*-helicity of 21° was still small enough to be compatible with the classification as barrel-stave supramolecule.[57] The NDI stacking in the *p*-octiphenyl turns of this widely open pore architecture was, however, possible only at the cost of some local distortion of the β-sheets. This local destabilization may account for the reduced inertness and apparent two-state behavior of pore **2** in single-pore conductance experiments (see below). Among several local minima, this particular architecture corresponds to the most stable conformer.

The minimal length of methylene spacer between β-sheet and NDI was found to determine the poor mobility of internal π-clamps. Nevertheless, the rotation of about 100° around the C_α–C_β single bond caused dramatic NDI movements to end up pointing toward the middle of the pore, where the π-stacks were again formed. In this second possible NDI architecture, the pore is closed. The observed high pore activity (see below), together with clearly poorer stability in molecular dynamics simulations, suggested that this closed NDI architecture is less favorable than the open architecture with NDI stacks next to the rigid-rod turns (Fig. 2).

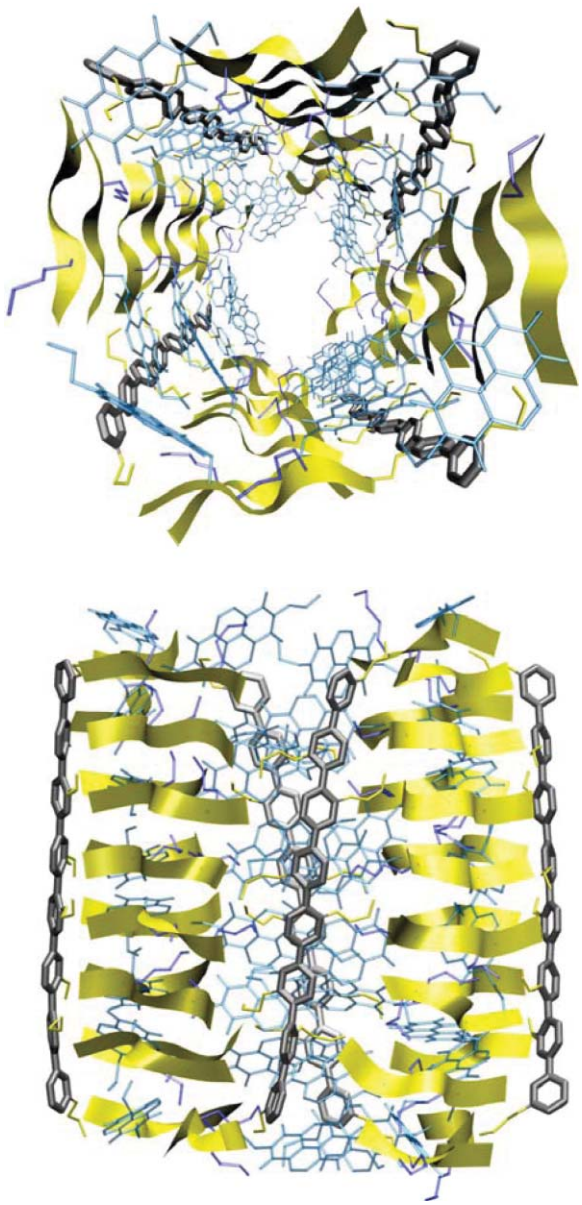

Fig. 2 Molecular dynamics simulations of synthetic multifunctional pore **2** in axial (*top*) and side view (*bottom*) with rigid-rod staves in dark gray, β-sheet hoops (ribbons) in yellow, lysine side-chains in blue (100% amine protonation) and NDI clamps in blue.

To simulate adhesive π-clamping within π-acidic pore **2**, the tetra-anionic version **3** of the π-basic dialkoxynaphthyl partner DAN in the classical DAN-NDI AEDA complexes was selected because of its excellent blockage efficiency and potential use for umami sensing (see below for experimental data and discussion). To π-clamp the DAN blocker, two of the NDIs initially folded back over *p*-octiphenyl turns are rotated around the C_α–C_β bond

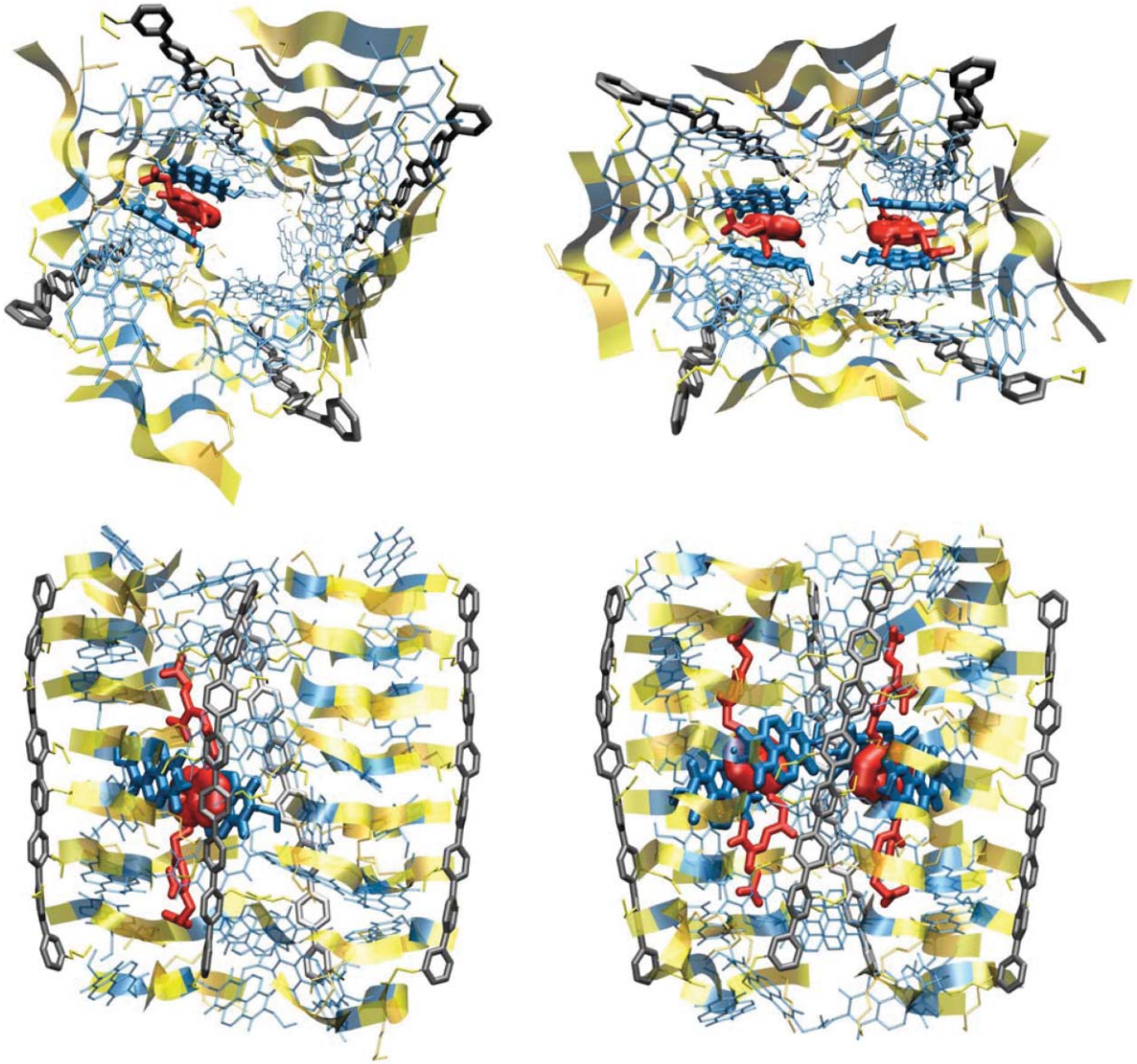

Fig. 3 Molecular dynamics simulations of pore-blocker complex **2** ⊃ **3** in axial (*top*) and side view (*bottom*) with one (**2** ⊃ $\mathbf{3}_1$, *left*) and two (**2** ⊃ $\mathbf{3}_2$, *right*) bound blockers **3** in red (100% carboxylic acid deprotonation). The rigid-rod staves of pore **2** are in dark grey, β-sheet hoops (ribbons) in orange (lysine, 100% amine protonation), yellow (leucine) and blue (NDI clamps).

of the sheet-clamp spacer. In the resulting, energy-minimized AEDA complex, the DAN blocker is caught between two sticky NDIs like a mosquito between two hands clapped together. The structures found after dynamics simulations were compatible with the existence of the experimentally confirmed adhesive π-clamping between DAN donor and NDI acceptors within **2** (Fig. 3). The carboxylate ion pairs with ammonium cations from surrounding lysines are embedded in a network of supportive hydrogen bonds.

The molecular dynamics simulations revealed the capacity of rigid-rod β-barrel **2** to accommodate in their internal space up to two DAN blockers. In the inclusion complex **2** ⊃ $\mathbf{3}_1$ with one DAN blocker, the pore experiences a small distortion, a guest → host template effect that preserves the *P*-helicity of 20° and contributes to the reduction of the minimal inner pore diameter to $d = 0.7$ nm. More pronounced guest → host template effects have been observed previously with rigid-rod β-barrels pores, both in computational models as well as in AFM images.[54,57] In the inclusion complex **2** ⊃ $\mathbf{3}_2$ with two DAN blockers, the minimal inner pore diameter further decreases to $d = 0.4$ nm. Both complexes are consistent with blockage of CF efflux, the observed Hill coefficients for DAN blockers are ambiguous, located consistently between $n = 1$ and $n = 2$ (see below).

Synthesis

Rigid rod **4** for self-assembly into pore **2** was synthesized from scratch in 23 steps overall (Scheme 1).[1] The *p*-octiphenyl scaffold **5** was prepared in nine steps from the commercially available biphenyl **6** and bromoacetate **7** following our optimized procedure without change.[63]

Several approaches to NDI amino acids have been reported previously.[64–66] We explored four different routes to synthesize NDI amino acid **8**. The best approach, in our hands, uses aspartate **9**, ethanolamine **10** and naphthalene dianhydride **11** as commercially available starting materials. The previously reported Hofmann rearrangement of aspartate **9** with iodosobenzene diacetate[67] provided facile and rapid access to Z-protected diaminopropionic acid (Dap) **12**. Reaction of Dap **12** with partially hydrolyzed dianhydride **11** under slightly acidic conditions afforded imide **13** in quantitative yield. The ethanolamine **14** with a removable TBDPS solubilizer was selected to introduce the second imide in NDI amino acid **8**. It was readily accessible from ethanolamine **10** in three simple steps.[68–70] Chemoselective Z-protection gave alcohol **15**, which was silylated to give **16**. Z-Deprotection afforded the desired amine **14**, reaction with diacid **13** produced the NDI amino acid **8** in 70% yield.

The solution-phase synthesis of tripeptide **17** was neither new[71,72] nor difficult. Attachment of the HBTU-activated NDI amino acid **8** following routine peptide synthesis procedures gave tetrapeptide **18**. Hydrogenolysis to deprotect the N-terminus afforded peptide **19**. Coupling with leucine **20** and deprotection of the N-terminus of NDI pentapeptide **21** with piperidine gave the key intermediate **22**.

Pentapeptide **22** was purified by semi-preparative HPLC before attachment to the freshly prepared *p*-octiphenyl **5**. Using 11.2 equivalents of pentapeptide **22**, 12 equivalents of HATU as coupling reagent and *N*,*N*-dimethylacetamide (DMA) as solvent, full conversion of octaacid **5** to peptide-rod conjugate **23** was accomplished within 1 h at room temperature in nearly quantitative yield. Removal of the TBDPS-solubilizers with HF–pyridine overnight at 0 °C (TBAF caused decomposition) followed by lysine deprotection with TFA gave the final rod **4**. The target molecule was purified by Sephadex LH-20 and reverse-phase HPLC before characterization and use. ESI MS, NMR spectra and RP-HPLC were all consistent with expected structure and sample homogeneity.

The key to the successful synthesis of NDI pore **2** was the introduction of TBDPS solubilizers. The NDI pentapeptide **22** with TBDPS was soluble in chloroform–methanol mixtures, DMF (>50 mg ml^{-1}) and *N*,*N*-dimethylacetamide (>100 mg ml^{-1}). The corresponding NDI pentapeptide **24** without TBDPS solubilizer was insoluble in chloroform–methanol mixtures and had low solubility in DMF (10–20 mg ml^{-1}) and *N*,*N*-dimethylacetamide (25–50 mg ml^{-1}, Fig. 4). The enormous usefulness of bulky spheres to solubilize difficult synthesis intermediates is well documented in the literature. The *tert*-butyl group in **7**, for example, has been the key for success in the initial synthesis of *p*-octiphenyl **5**.[73]

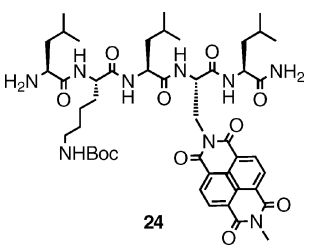

Fig. 4 Structure of NDI pentapeptide **24**, similar to **22** but without TBDPS solubilizers (synthesis not shown).

Pore activity in fluorogenic vesicles

Arguably the simplest and most reliable approach to zoom in on activity and selectivity of synthetic ion channels and pores begins with the determination of pH profile and Hill plot in fluorogenic vesicles.[17–32] Egg yolk phosphatidylcholine large unilamellar vesicles loaded with fluorophore 8-aminonaphthalene-1,3,6-trisulfonate and quencher *p*-xylene-bis-pyridinium bromide (EYPC-LUVs ⊃ ANTS–DPX) were used to measure the pH profile of pore **2**. In the ANTS–DPX assay, pore activity is observed as an increase in ANTS emission due to efflux of the cationic quencher DPX, the anionic fluorophore ANTS, or both. This assay is ideal to record pH profiles because of the poor sensitivity to pH changes and the ion selectivity of the pore.[53,74] This is important because it assures that the reported changes really originate from changes in the activity of the pore with pH and not from changes in the ion selectivity of the pore with pH or changes in the properties of the assay itself with pH.

The pH profile revealed that pore **2** closes at high pH as expected for pore collapse without internal charge repulsion between at least partially protonated lysine amines (Fig. 5, effective $pH_{50} = 8.8$).[74–76] However, different to pore **1**, pore **2** was insensitive to acid. This finding confirmed the suspicion that in pore **1**, partially or fully protonated histidines (intrinsic $pK_a \sim 6$) are responsible for the charge repulsion leading to full opening of pore around pH 5 or inactivation by overcharging at pH < 5, respectively.[53,74–76] This additional possibility to charge and overcharge pores disappears with the replacement of these histidines in pore **1** with the NDI clamps in pore **2**. Acid insensitivity, therefore, suggested that pore **2** may be permanently undercharged and never reach full activity. This interpretation was in agreement with decreasing activity with increasing ionic strength (Fig. 6).

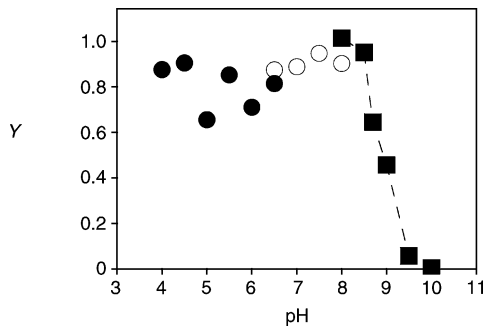

Fig. 5 pH profile of pore **2**. Fractional ANTS emission intensity *Y* (λ_{ex} 353 nm, λ_{em} 510 nm) 4 min after the addition of monomer **4** (200 nM final) to EYPC-LUVs ⊃ ANTS–DPX [~125 μM EYPC; inside: 12.5 mM ANTS, 45 mM DPX, 5 mM TES, 20 mM NaCl, pH 7; outside: 100 mM NaCl, 10 mM MES (●), HEPES (○) or AMPSO (■)] as a function of pH (25 °C, calibrated by final lysis).

The concentration dependence of pore activity[53,55,77] was determined in EYPC-LUVs ⊃ CF. Similar to the ANTS–DPX assay, pore activity in the CF assay is reported as an increase in CF emission, because CF dilution by CF efflux from the vesicles reduces CF self-quenching. Compared to the ANTS–DPX assay, the CF assay is cheaper and more sensitive but has limited applicability to anion-transporting large pores and works at pH ≥ 6.5 only. The Hill plot of pore **2** revealed non-linear dependence of pore activity on the concentration of monomer **4**

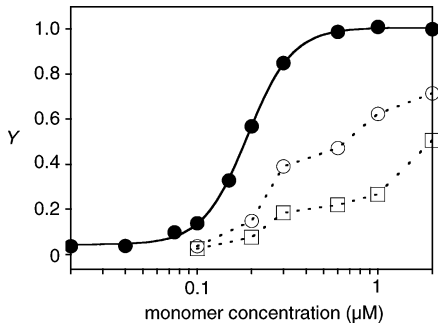

Fig. 6 Hill plot of pore **2** with dependence on ionic strength [107 mM (●), 200 mM (○) and 300 mM NaCl (□)]. Fractional CF emission intensity Y (λ_{ex} 492 nm, λ_{em} 517 nm) 4 min after the addition of monomer **4** (0–2 μM final) to EYPC-LUVs ⊃ CF [~125 μM EYPC, 10 mM HEPES; inside: 50 mM CF, pH 7.4, X-100 mM NaCl; outside: pH 6.5, X mM NaCl, X = 107 (●), 200 (○) or 300 (■)] as a function of the concentration of monomer **4** (25 °C, calibrated by final lysis).

(Fig. 6●). This demonstrated that more than one rod **4** is needed to form an active pore, *i.e.*, the presence of supramolecular function. The observed Hill coefficient $n = 3.5 \pm 0.1$ was compatible with tetramer **2**, a contracted trimer, a mixture of both, or, naturally, the average of any more complex mixture. The non-linear Hill plot further demonstrated that the self-assembly of pore **2** is endergonic.[53,55] Thermodynamic instability and tri- to tetrameric active suprastructure of pore **2** were as with pore **1**. With an effective concentration $EC_{50} = 47.5 \pm 0.5$ nM (*i.e.*, 190 ± 2 nM monomer **4**), tetramer **2** was about one order of magnitude more active than tetramer **1** and overall one of the most active rigid-rod β-barrel pores reported so far. For reasons discussed elsewhere,[53] high activity coupled with thermodynamic instability are ideal characteristics for sensing applications.

The activity of pore **2** decreased with increasing ionic strength. The effective concentration $EC_{50} = 47.5 \pm 0.5$ nM for tetramer **2** in 107 mM NaCl increased to $EC_{50} \approx 170$ nM in 200 mM NaCl (Fig. 6○) and $EC_{50} \approx 500$ nM in 300 mM NaCl (Fig. 6□). This salt effect was consistent with sensitivity to base because both increasing ion pairing and deprotonation decrease internal charge repulsion. Higher sensitivity of pore **2** to ionic strength compared to pore **1** was thus in support of the comparably poor internal charge repulsion. Ongoing attempts to treat the dependence of pore activity on ionic strength quantitatively[76,78] were so far not as successful as with pH profiles.[74,75]

The Hill coefficients of pore **2** decreased with increasing ionic strength. This trend could originate from increasing incompatibility with Hill analysis as the monomer concentration decreases with increasing thermodynamic pore stability in response to decreasing internal charge repulsion.[55,74,76] This interpretation was in agreement with the suspicion that a closed, inactive barrel without internal charge repulsion is more stable than an internally charged, open and active barrel. The stabilization of internal space by intermediate internal charge repulsion may thus necessarily destabilize the pore itself and require counter pressure from the surrounding membrane to exist.[76]

Planar bilayer conductance

The addition of rod **4** to planar EYPC membranes caused the appearance of rather heterogeneous single-pore currents (Fig. 7).

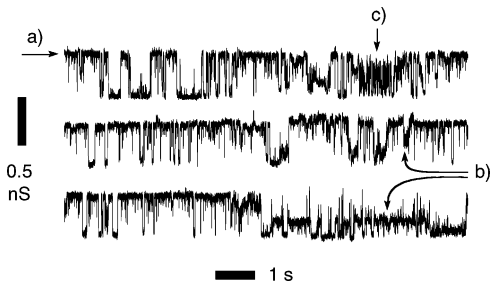

Fig. 7 Representative planar EYPC bilayer conductance in the presence of rod **4** (0.08 mol%) at +50 mV in 2 M KCl. Conductance levels include a) high conductance with a long lifetime, b) several lower conductance levels and c) frequent high conductance with a very short lifetime.

One dominant current level was relatively long-lived and had the high conductance expected for the large inner diameter of rigid-rod β-barrel **2** with internal NDI oriented along the *p*-octiphenyl scaffolds (Fig. 7a, 1 and 2). Many interpretations for the observable levels of lower conductance were conceivable, including reduction of the apparent internal diameter by NDIs oriented toward the center of the pore (Fig. 7b and 1). A high-conducting rapid flickering occurred quite frequently (Fig. 7c). The similarity in high conductance between these very labile single-pore currents and the very inert single-pore currents mentioned above was reminiscent of the Engelman two-state model,[79] where the formation of the inert rigid-rod β-barrel **2** would be preceded by a labile bundle of transmembrane rods of similar structure but without the stabilizing β-sheets. Similar observations in support of a two-state model have been made previously.[80] Molecular dynamics simulations confirmed that internal NDI clamps may destabilize and distort the β-sheets of the rigid-rod β-barrel (Fig. 2).

While the appearance of single-pore currents was well reproducible, their characteristics could change from experiment to experiment without a clear pattern. The observed comparably high heterogeneity may indicate that the introduction of internal NDI clamps increases the number of different active suprastructures, either by the β-sheet destabilization indicated by Engelman-type two-state behavior and molecular dynamics simulations, the accumulation of otherwise imperfect barrels, barrel contraction into trimers or flattened tetramers,[54] or large motions of internal NDIs within otherwise perfect rigid-rod β-barrels (Fig. 1). In any case, further investigation and (over)interpretation was not meaningful at this stage given the complexity of the single-pore characteristics. Perhaps because of their dynamic, adaptable suprastructure, rigid-rod β-barrel pores with irregular single-pore characteristics were identified previously as excellent optical transducers of chemical reactions, enzyme detectors and biosensors.[18,81] Results described in the following sections are similarly promising.

Nucleotide recognition

Nucleotide recognition is an ideal topic for π-clamping because their central role in biology promises many applications, from multicomponent sensing in complex matrixes[18–20] to gene sequencing with pores.[82–84] Previous approaches to nucleotide clamping include Schneider's porphyrin clefts[5] and Waters' elegant β-hairpins.[15,16] Interestingly, previous examples of nucleotide recognition by synthetic[20] and bioengineered[84] pores on the one hand and by NDIs on the other hand[85] do not operate on π-clamping.

Table 1 Nucleotide recognition by pores **1** and **2**

	Blocker[a]	Ionic strength[b]	IC_{50} (**2**)/μM[c]	IC_{50} (**1**)/μM[c]	Π[d]
1	ATP	+	14	22[e]	1.6
2	ATP	++	21	131[e]	6.2
3	ADP	+	83	224[e]	2.7
4	AMP	+	1062	8100	7.6
5	AMP	++	938	9000	9.6
6	GTP	++	22	73	3.3
7	GDP	+	77	—[f]	
8	GMP	+	1055	—[f]	
9	GMP	++	967	—[f]	
10	CDP	+	505	—[f]	
11	UDP	+	488	—[f]	

[a] Nucleotides (three-letter abbreviations). [b] Outside: 107 mM NaCl (+) or 200 mM NaCl (++), 10 mM HEPES, pH 6.5; inside: 10 mM NaCl (+) or 100 mM NaCl (++), 50 mM CF, 10 mM HEPES, pH 6.5. [c] Nucleotide concentration required for 50% blockage, determined from fluorogenic CF efflux from EYPC-LUVs ⊃ CF (see Fig. 8 and 9). [d] Clamping factor Π = IC_{50} (**1**)/IC_{50} (**2**). [e] Data from ref. 20. [f] Not determined.

Nucleotide recognition by pore **2** with internal NDI π-clamps was monitored with the CF assay. An original trace is shown in Fig. 8, where addition of pore **2** at t = 30 seconds is followed by a dramatic increase in CF emission. To determine molecular recognition with this assay on molecular translocation of CF, the same experiment was repeated in the presence of the analyte of interest, *e.g.*, ATP (Fig. 8). The observed increasing hindrance of CF efflux with increasing concentration of ATP is exactly what is expected from π-clamping of ATP within pore **2**. Hill analysis of the dose response curves for ATP gave IC_{50} = 14 μM in 107 mM NaCl and IC_{50} = 21 μM in 200 mM NaCl (Table 1, entries 1 and 2, Fig. 9◆). ATP recognition by pore **2** was more than three orders of magnitude better than ion-pair assisted ATP recognition by tryptophan clamps on one side of a synthetic β-sheet (K_D = 48 000 μM, 200 mM KCl).[15]

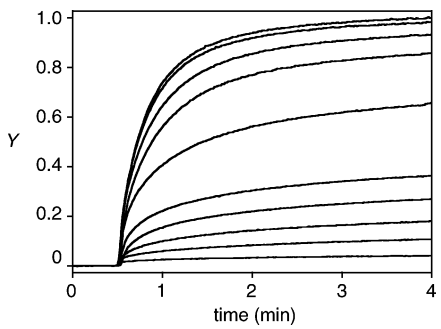

Fig. 8 Blockage of pore **2** by ATP. Fractional change in CF emission Y (λ_{ex} 492 nm, λ_{em} 517 nm) as a function of time after addition of ATP (top down: 0, 1, 3, 5, 10, 20, 30, 50, 100 and 500 μM) and monomer **4** (200 nM (at $t \sim 30$ s) to EYPC-LUVs ⊃ CF (∼125 μM EYPC, 10 mM HEPES; inside: 50 mM CF, pH 7.4, 10 mM NaCl; outside: pH 6.5, 107 mM NaCl), calibrated with final addition of excess triton X-100.

The clamping factor Π = IC_{50} (**1**)/IC_{50} (**2**) was introduced to quantify isolate contributions from π-clamping within pore **2** by comparison with the π-clamp-free pore **1**. The clamping factor Π = 1.6 for ATP recognition at lower ionic strength was poor (Table 1, entry 1), perhaps also because of emerging interference from stoichiometric binding at low IC_{50}s.[86] It increased to a more

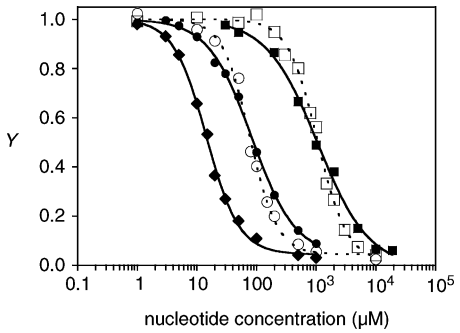

Fig. 9 Dose response curves for the blockage of pore **2** (200 nM monomer **4**) by ATP (◆), ADP (●), AMP (■), GDP (○) and GMP (□). Conditions as in Fig. 8, ionic strength, 107 mM NaCl (Table 1, +).

significant Π = 6.2 at higher ionic strength (Table 1, entry 2). An increasing clamping factor with increasing ionic strength was consistent with an increasing dominance of π-clamping over ion pairing under these conditions.

The discrimination of ATP and ADP is important for sensing applications because it assures detectability of all ATP-dependent processes.[20] Compared to the ADP/ATP discrimination factor D = IC_{50}(ADP)/IC_{50}(ATP) = 10.2 for pore **1**, the introduction of π-clamps within pore **2** reduced D to 5.9 (Table 1, entry 1 *vs.* 3; Fig. 9, ◆ *vs.* ●). This result was as expected for interference of constant contributions from π-clamping with sensitivity toward changes in ion pairing. However, an excellent D = 11.8 was reported for Waters' β-hairpin π-clamps at low ionic strength,[15] and pore **1** gave up to D = 18.0 at low ionic strength.[20]

Moving from ADP to AMP, IC_{50}s further increased for both pores **1** and **2** (Table 1, entries 3–5; Fig. 9, ● *vs.* ■). Contributions from π-clamping were, however, most relevant at reduced ion pairing with AMP. Clamping factors Π = 7.6 at lower and Π = 9.6 at higher ionic strength were clearly better than those with ATP. Clamping factors for AMP thus still increased with ionic strength, although the trend was less pronounced than with ATP. As a result, IC_{50}s for AMP recognition by pore **2** *decreased* with ionic strength, whereas IC_{50}s for AMP recognition by π-clamp-free pore **1** *increased* with ionic strength. Although a small effect, this increasing recognition with increasing ionic strength provided quite remarkable direct experimental evidence for the existence and power of π-clamping within pore **2**. Identical results for GMP confirmed the general relevance of this finding (Table 1, entries 8 and 9).

The discrimination of purines and pyrimidines by π-clamp pore **2** was as unproblematic as expected. Already at low ionic strength, molecular recognition of both ADP and GDP was about 6-times better than that of CDP and UDP (Table 1, entries 3, 7, 10 and 11). This difference was in the range of that reported for β-hairpin π-clamps.[15] Naturally, this result was in support of effective π-clamping within pore **2**.

Discrimination between different purines by *e.g.*, contributions from aromatic donor–acceptor interactions to π-clamping within pore **2**, was less obvious. The IC_{50}s for ANPs and GNPs at low ionic strengths were overall almost the same (Table 1; Fig. 9, ●■ *vs.* ○□). The difference of the redox potentials is possibly too small (G: 1.29 V, A: 1.42 V *vs.* NHE at pH 7)[87] for substantial contributions from aromatic donor–acceptor interactions with the π-acidic NDI clamps. The higher cooperativity found in the

dose response curves for GNP compared to ANP recognition suggested that purine recognition by π-clamp pore **2** is dominated by phenomena beyond charge-transfer complexation (Fig. 9, ●■ *vs.* ○□; G: $n \approx 1.8$, A: $n \approx 1.1$). We are currently exploring the possibility of contributions from G-quartet[29,88,89] formation to this poorly understood effect. The often more complex trends found for nucleobase discrimination by related systems such as porphyrin tweezers[5] or synthetic β-hairpins[15,16] are in agreement with these observations.

Adhesive π-clamping

The terms "adhesive " or "sticky" are for π-clamps that can use aromatic electron donor–acceptor interactions (AEDA) to catch analytes. To systematically explore the existence of adhesive π-clamping within the π-acidic pore **2**, the π-basic dialkoxynaphthalene (DAN)[33–37,43] intercalators **3**, **25** and **26**, π-acidic NDI intercalators **27–29** and the non-aromatic control **30** were synthesized (Scheme 2).[1] A modular approach for rapid blocker screening with DAN hydrazide **31**, NDI hydrazide **32** and adipic dihydrazide **33** was conceived for future use in sensing applications. Reaction of these π-acidic, π-basic and non-aromatic scaffolds with ketones of various size and charge[90–95] was expected to provide facile access to quantitative insights on adhesive π-clamping within pore **2**. Pyruvate **34** and α-ketoglutarate **35** were selected as representative analytes of diagnostic interest. The hydrazones **3**, **26**, and **28–30** obtained by *in situ* reaction with hydrazides **31–33** under mildly acidic conditions were expected to be stable under neutral and basic conditions.[90–95]

DAN hydrazide **31** was prepared from the commercially available naphthalene **36** by Williamson ether synthesis with methyl bromoacetate **37** followed by the reaction of ester **38**[96] with hydrazine. Williamson ether synthesis of naphthalene **36** with *t*-butyl bromoacetate **7** for mild hydrolysis of ester **39** with TFA was used to prepare DAN diacid **3**.[96]

NDI hydrazide **32** was synthesized from dianhydride **11** and Z-protected β-alanine **40**. Procedures for the conversion of the latter into the Boc-protected hydrazide **41** followed by hydrogenolytic amine deprotection are available in the literature.[97] Reaction of amine **42** with dianhydride **11** afforded diimide **43**, which was readily deprotected with TFA. Reaction of dianhydride **11** with β-alanine **44** afforded NDI diacid **27** in one step.[98]

The efficiency of this series of DAN and NDI intercalators to block pore **2** and π-clamp-free control pore **1** was determined from the inhibition of the fluorogenic efflux of CF from EYPC-LUVs ⊃ CF as described above for nucleotides (compare Fig. 8 and 9). The results provided remarkably consistent evidence for the occurrence and significance of adhesive π-clamping within pore **1** (Table 2). As for nucleotides, contributions from ion pairing were the easiest to identify: IC_{50}s decreased with increasing negative

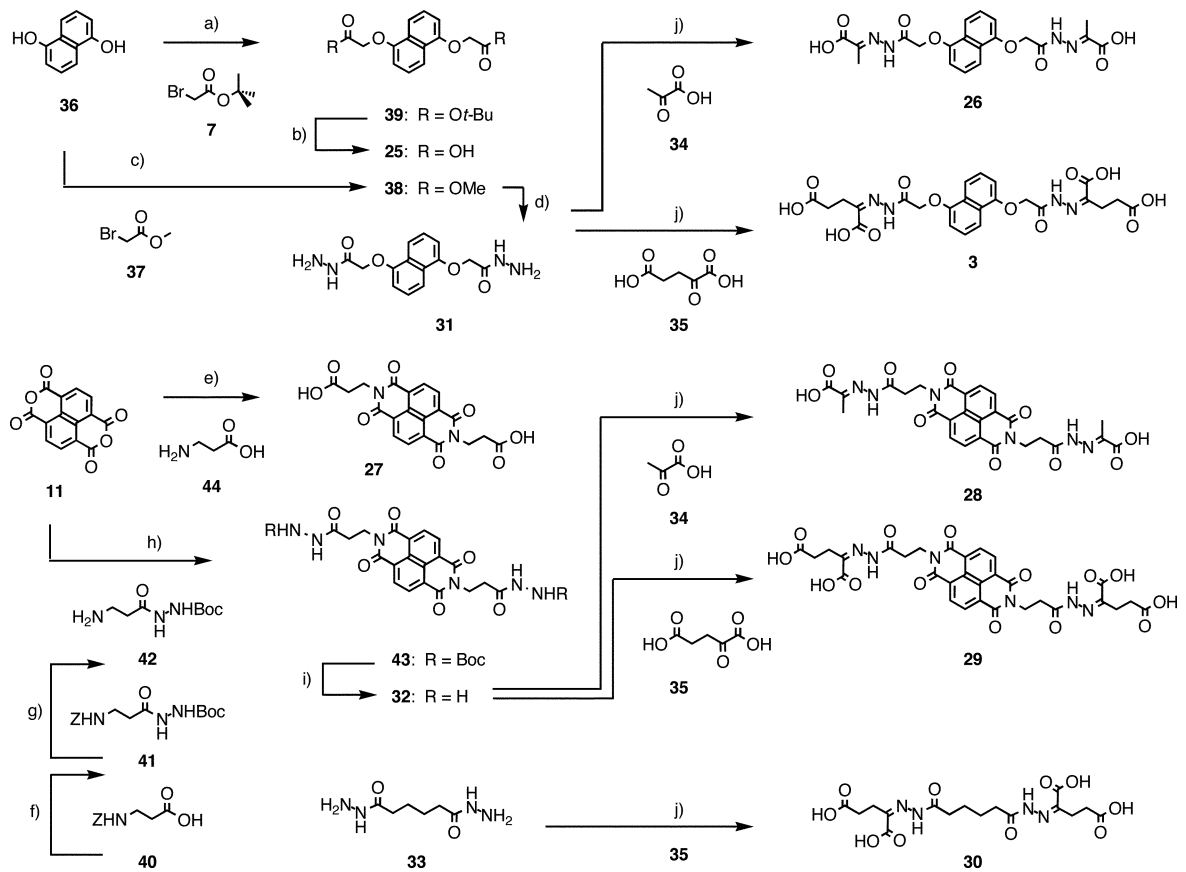

Scheme 2 Synthesis of NDI and DAN modules for *in situ* screening of pore blockers. (a) Cs_2CO_3, acetone, reflux. (b) TFA, quant.[96] (c) Cs_2CO_3, acetone, reflux, 77%.[96] (d) NH_2NH_2, EtOH, reflux, 12 h, quant. (e) 135 °C, 3 d, 93%.[98] (f) NH_2NHBoc, HBTU, CH_2Cl_2, 0 °C–rt, 1 h, 63%.[97] (g) $Pd(OH)_2/C$, H_2, MeOH, quant.[97] (h) DMF, 90 °C, 12 h, 81%. (i) TFA, 89%. (j) Ketone–hydrazide = 1 : 10, DMSO, 2 h, 50 °C.

Table 2 Adhesive π-clamping within pore **2**[a,b,1]

	Blocker[c]	Formal charge	IC_{50} (**2**)/μM[d]	IC_{50} (**1**)/μM[d]	Π[e]	Π_{DA}[f]
1	**25**	−2	94.7	2043	21.6	4.8
2	**26**	−2	4.5	136	30.3	3.9
3	**3**	−4	0.24	9.8	40.8	3.8
4	**27**	−2	32.7	147	4.5	
5	**28**	−2	25.7	197	7.7	
6	**29**	−4	2.5	26.9	10.8	
7	**30**	−4	>100	–[g]		

[a] Data from ref. 1. [b] Determined from dose response curves for fluorogenic CF efflux from EYPC-LUVs ⊃ CF, compare Fig. 8 and 9. [c] See Scheme 2 for structures. [d] Blocker concentration required for 50% blockage. Data are the average value of at least three independent measurements, standard error mostly <5%, always <10%. [e] Clamping factor $\Pi = IC_{50}$ (**1**)/IC_{50} (**2**). [f] Donor–acceptor factor $\Pi_{DA} = \Pi_D/\Pi_A$; *e.g.*, Π_{DA} (entry 1) = Π (**25**)/Π (**27**). [g] Not determined.

charge of aromatic blockers. Remarkably, the aliphatic hydrazone **30** did not block pore **2** at all despite its high charge. Significant contributions from π-clamping were revealed by clamping factors reaching from $\Pi = 4.5$ for the small NDI dianion **27** up to a remarkable $\Pi = 40.8$ for the large DAN tetraanion **3** (Table 2, entries 3 and 4). The "assistance" of ion pairing to maximize π-clamping was confirmed by increasing clamping factors Π with increasing blocker charge. The adhesiveness of π-clamping within pore **2**, that is, the existence of aromatic electron donor–acceptor interactions, was revealed by comparison of clamping factors Π for π-basic DANs and π-acidic NDIs. Clamping factors up to $\Pi = 10$ for the π-acidic NDI intercalators **27–29** were in the range found for nucleotides. The clamping factors between $\Pi = 20$ and $\Pi = 40$ for the π-basic DAN intercalators **3**, **25** and **26** exceeded this range by far. The observed donor–acceptor factors $\Pi_{DA} \approx 4$ were roughly independent of intercalator size and charge (Table 2, entries 1–3).

The identified donor–acceptor factors $\Pi_{DA} \approx 4$ provided surprisingly clear-cut experimental evidence for the existence of significant contributions from aromatic electron donor–acceptor interactions to molecular recognition within pore **2**. Most importantly, the findings demonstrate that adhesive π-clamping provides access to molecular recognition not only with high sensitivity but also with high selectivity. This evidence for operational sticky π-clamps was in agreement with results from molecular dynamics simulations (Fig. 2 and 3). Experimental insights concerning cooperativity were less convincing. The observed Hill coefficients for blockage of pore **2** by pertinent DAN and NDI blockers **3**, **26**, **28** and **29** were in the range of $n = 1.1$–1.5. Although not very convincing, this result suggested that more than one blocker may be needed to block pore **2**. With minimal internal pore diameters of $d = 0.7$ nm with one and $d = 0.4$ nm with two DAN blockers **3**, results from molecular dynamics simulations were less ambiguous with regard to cooperativity (Fig. 3). Consistently higher Hill coefficients $n = 1.4$–2.2 were found for blockage of the less crowded pore **1** with the same blockers.

Conclusions

The substantial synthetic efforts required to introduce artificial amino acids at the inner surface of rigid-rod β-barrels to create pores with sticky π-clamps were fully rewarded. The reported findings demonstrate that adhesive π-clamping provides access to molecular recognition not only with high sensitivity but also with high selectivity. This breakthrough is important for the application of synthetic pores as sensors.

As far as the characteristics of the new pore as such are concerned, insensitivity to acid but closing at high pH and high ionic strength were identified. Hill plot and single pore conductance reveal the dynamic characteristics of an unstable, tri- to tetrameric pore that are of interest for practical sensing applications.

Molecular dynamics simulations revealed that empty naphthalenediimide (NDI) clamps within tetrameric pores can open up sideward to cover the rigid-rod staves and leave the internal space free for unhindered translocation of molecules as large as carboxyfluorescein. Molecular modeling further suggested that these "open" NDI clamps could flip inward to firmly catch matching analytes passing by.

π-Clamping within the new pore was explored with nucleotides, π-basic and π-acidic naphthalenes and aliphatic controls. Nucleotide clamping was characterized by excellent sensitivity (orders of magnitude beyond similar systems), excellent discrimination of purines over pyrimidines, modest discrimination between different charges (ATP *vs.* ADP) and poor discrimination between different purines (ATP *vs.* GTP).

The introduction of π-basic DAN, π-acidic NDI and non-aromatic dihydrazide scaffolds provided access to a convenient screening approach of blocker libraries. Pyruvate and α-ketoglutarate hydrazones as representative analytes of biological significance were already sufficient to secure experimental evidence for all aspects of adhesive π-clamping, including assistance from ion pairing and relevance of aromatic electron donor–acceptor interactions.

The availability of refined pores for molecular recognition beyond ion pairing on one hand and hydrazone scaffolds for rapid analyte screening on the other are exceptionally promising with regard to practical applications of synthetic pores as sensors. Studies on multicomponent sensing in complex matrixes with sticky π-clamps within synthetic pores and the synthesis of pores with either more slippery or more flexible π-clamps are ongoing.

Acknowledgements

We thank D. Jeannerat, A. Pinto and S. Grass for NMR spectroscopy measurements, P. Perrottet and the group of F. Gülaçar for MS measurements, the Swiss National Supercomputing Center in Manno for CPU time on their CRAY-XT3 computer, the

referees for their assistance in improving the quality of the manuscript, and the Swiss NSF for financial support.

References

1 H. Tanaka, S. Litvinchuk, G. Bollot, J. Mareda, D.-H. Tran, N. Sakai and S. Matile, *J. Am. Chem. Soc.*, 2006, **128**, 16000–16001.
2 C.-W. Chen and H. W. Whitlock, *J. Am. Chem. Soc.*, 1978, **100**, 4921–4922.
3 A. E. Rowan, J. A. A. W. Elemans and R. J. M. Nolte, *Acc. Chem. Res.*, 1999, **32**, 995–1006.
4 F. G. Klärner and B. Kahlert, *Acc. Chem. Res.*, 2003, **36**, 919–932.
5 H.-J. Schneider, L. Tianjun, M. Sirish and V. Malinovski, *Tetrahedron*, 2002, **58**, 779–786.
6 D. Sun, F. S. Tham, C. A. Reed, L. Chaker and P. D. W. Boyd, *J. Am. Chem. Soc.*, 2002, **124**, 6604–6612.
7 A. T. Charlton, A. L. Davis, D. P. Jones, J. R. Lewis, A. P. Davis, E. Haslam and M. P. Williamson, *J. Chem. Soc., Perkin Trans. 2*, 2000, 317–322.
8 S. C. Zimmerman and K. W. Saionz, *J. Am. Chem. Soc.*, 1995, **117**, 1175–1176.
9 H. M. Colquhoun, Z. Zhu and D. J. Williams, *Org. Lett.*, 2003, **5**, 4353–4356.
10 T. Korenaga, Y. Kawauchi, T. Kosaki, T. Ema and T. Sakai, *Bull. Chem. Soc. Jpn.*, 2005, **78**, 2175–2179.
11 S. Yagi, M. Ezoe, I. Yonekura, T. Takagishi and H. Nakazumi, *J. Am. Chem. Soc.*, 2003, **125**, 4068–4069.
12 X. Huang, K. Nakanishi and N. Berova, *Chirality*, 2000, **12**, 237–255.
13 Y. Shoji, K. Tashiro and T. Aida, *J. Am. Chem. Soc.*, 2006, **128**, 10690–10691.
14 J. M. Kerckhoffs, M. G. ten Cate, M. A. Mateos-Timoneda, F. W. van Leeuwen, B. Snellink-Ruel, A. L. Spek, H. Kooijman, M. Crego-Calama and D. N. Reinhoudt, *J. Am. Chem. Soc.*, 2005, **127**, 12697–12708.
15 S. M. Butterfield and M. L. Waters, *J. Am. Chem. Soc.*, 2003, **125**, 9580–9581.
16 S. M. Butterfield, M. M. Sweeney and M. L. Waters, *J. Org. Chem.*, 2005, **70**, 1105–1114.
17 N. Sakai, J. Mareda and S. Matile, *Acc. Chem. Res.*, 2005, **38**, 79–87.
18 G. Das, P. Talukdar and S. Matile, *Science*, 2002, **298**, 1600–1602.
19 G. Das and S. Matile, *Chem.–Eur. J.*, 2006, **12**, 2936–2944.
20 S. Litvinchuk, N. Sordé and S. Matile, *J. Am. Chem. Soc.*, 2005, **127**, 9316–9317.
21 Y. Baudry, D. Pasini, M. Nishihara, N. Sakai and S. Matile, *Chem. Commun.*, 2005, **40**, 4798–4800.
22 P. Scrimin and P. Tecilla, *Curr. Opin. Chem. Biol.*, 1999, **3**, 730–735.
23 G. W. Gokel and A. Mukhopadhyay, *Chem. Soc. Rev.*, 2001, **30**, 274–286.
24 U. Koert, L. Al-Momani and J. R. Pfeifer, *Synthesis*, 2004, **8**, 1129–1146.
25 S. Matile, A. Som and N. Sordé, *Tetrahedron*, 2004, **60**, 6405–6435.
26 A. L. Sisson, M. R. Shah, S. Bhosale and S. Matile, *Chem. Soc. Rev.*, 2006, **35**, 1269–1286.
27 T. M. Fyles, *Chem. Soc. Rev.*, 2007, **36**, 335–347.
28 A. P. Davis, D. N. Sheppard and B. D. Smith, *Chem. Soc. Rev.*, 2007, **36**, 348–357.
29 J. T. Davis and G. P. Spada, *Chem. Soc. Rev.*, 2007, **36**, 296–313.
30 Y. Kobuke, K. Ueda and M. Sokabe, *J. Am. Chem. Soc.*, 1992, **114**, 7618–7622.
31 W.-H. Chen, X.-B. Shao and S. L. Regen, *J. Am. Chem. Soc.*, 2005, **127**, 12727–12735.
32 F. Otis, N. Voyer, A. Polidori and B. Pucci, *New J. Chem.*, 2006, **30**, 185–190.
33 R. S. Lokey and B. L. Iverson, *Nature*, 1995, **375**, 303–305.
34 G. J. Gabriel and B. L. Iverson, *J. Am. Chem. Soc.*, 2002, **124**, 15174–15175.
35 S. A. Vignon, T. Jarrosson, T. Iijima, H. R. Tseng, J. K. M. Sanders and J. F. Stoddart, *J. Am. Chem. Soc.*, 2004, **126**, 9884–9885.
36 P. Mukhopadhyay, Y. Iwashita, M. Shirakawa, S. Kawano, N. Fujita and S. Shinkai, *Angew. Chem., Int. Ed.*, 2006, **45**, 1592–2595.
37 P. Talukdar, G. Bollot, J. Mareda, N. Sakai and S. Matile, *J. Am. Chem. Soc.*, 2005, **127**, 6528–6529.
38 V. Gorteau, G. Bollot, J. Mareda, A. Perez-Velasco and S. Matile, *J. Am. Chem. Soc.*, 2006, **128**, 14788–14789.
39 L. L. Miller and K. R. Mann, *Acc. Chem. Res.*, 1996, **29**, 417–423.
40 H. E. Katz, A. J. Lovinger, J. Johnson, C. Kloc, T. Siegrist, W. Li, Y. Y. Lin and A. Dodabalapur, *Nature*, 2000, **404**, 478–481.
41 J. Lee, V. Guelev, S. Sorey, D. W. Hoffman and B. L. Iverson, *J. Am. Chem. Soc.*, 2004, **126**, 14036–14042.
42 S. Bhosale, A. L. Sisson, P. Talukdar, A. Fürstenberg, N. Banerji, E. Vauthey, G. Bollot, J. Mareda, C. Röger, F. Würthner, N. Sakai and S. Matile, *Science*, 2006, **313**, 84–86.
43 S. Bhosale, A. L. Sisson, N. Sakai and S. Matile, *Org. Biomol. Chem.*, 2006, **4**, 3031–3039.
44 S. H. White and G. von Heijne, *Curr. Opin. Struct. Biol.*, 2005, **15**, 378–386.
45 W. M. Yau, W. C. Wimley, K. Gawrisch and S. H. White, *Biochemistry*, 1998, **37**, 14713–14718.
46 M. R. R. De Planque, B. B. Bonev, J. A. A. Demmers, D. V. Greathouse, R. E. Koeppe, II, F. Separovic, A. Watts and J. A. Killian, *Biochemistry*, 2003, **42**, 5341–5348.
47 J. M. Sanderson, *Org. Biomol. Chem.*, 2005, **3**, 201–212.
48 B. A. Krantz, R. A. Melnyk, S. Zhang, S. J. Juris, D. B. Lacy, Z. Wu, A. Finkelstein and R. J. Collier, *Science*, 2005, **309**, 777–781.
49 D. A. Doyle, J. M. Cabral, R. A. Pfuetzner, A. Kuo, J. M. Gulbis, S. L. Cohen, B. T. Chait and R. MacKinnon, *Science*, 1998, **280**, 69–77.
50 S. Khademi, J. O'Connell, III, J. Remis, Y. Robles-Colmenares, L. J. W. Miercke and R. M. Stroud, *Science*, 2004, **305**, 1587–1594.
51 A. Okada, T. Miura and H. Takeuchi, *Biochemistry*, 2001, **40**, 6053–6060.
52 X. Guan, L.-Q. Gu, S. Cheley, O. Braha and H. Bayley, *ChemBioChem*, 2005, **6**, 1875–1881.
53 S. Litvinchuk, G. Bollot, J. Mareda, A. Som, D. Ronan, M. R. Shah, P. Perrottet, N. Sakai and S. Matile, *J. Am. Chem. Soc.*, 2004, **126**, 10067–10075.
54 J. Kumaki, E. Yashima, G. Bollot, J. Mareda, S. Litvinchuk and S. Matile, *Angew. Chem., Int. Ed.*, 2005, **44**, 6154–6157.
55 S. Bhosale and S. Matile, *Chirality*, 2006, **18**, 849–856.
56 B. Baumeister and S. Matile, *Chem. Commun.*, 2000, **35**, 913–914.
57 V. Gorteau, G. Bollot, J. Mareda, D. Pasini, D.-H. Tran, A. N. Lazar, A. W. Coleman, N. Sakai and S. Matile, *Bioorg. Med. Chem.*, 2005, **13**, 5171–5180.
58 *MacroModel 7.0*, Schrödinger Inc., Portland, OR, 1999.
59 F. Mohamadi, N. G. J. Richards, W. C. Guida, R. Liskamp, M. Lipton, C. Caufield, G. Chang, T. Hendrickson and W. C. Still, *J. Comput. Chem.*, 1990, **11**, 440–467.
60 *Maestro 4.1*, Schrödinger Inc., Portland, OR, 2001.
61 T. A. Halgren, *J. Comput. Chem.*, 1999, **20**, 720–748.
62 D. A. Case, T. A. Darden, T. E. Cheatham, III, C. L. Simmerling, J. Wang, R. E. Duke, R. Luo, K. M. Merz, B. Wang, D. A. Pearlman, M. Crowley, S. Brozell, V. Tsui, H. Gohlke, J. Mongan, V. Hornak, G. Cui, P. Beroza, C. Schafmeister, J. W. Caldwell, W. S. Ross and P. A. Kollman, *AMBER 8*, University of California, San Francisco, 2004.
63 B. Baumeister, N. Sakai and S. Matile, *Org. Lett.*, 2001, **3**, 4229–4232.
64 T. Wagner, W. B. Davis, K. B. Lorenz, M. E. Michel-Beyerle and U. Diederichsen, *Eur. J. Org. Chem.*, 2003, 3673–3679.
65 A. A. Mokhir and R. Kraemer, *Bioconjugate Chem.*, 2003, **14**, 877–883.
66 N. Ashkenasy, W. S. Horne and M. R. Ghadiri, *Small*, 2006, **1**, 99–102.
67 L. Zhang, G. S. Kauffman, J. A. Pesti and J. Yin, *J. Org. Chem.*, 1997, **62**, 6918–6920.
68 S. Hanessian and P. LaVallee, *Can. J. Chem.*, 1975, **53**, 2975–2977.
69 D. Wenninger and H. Seliger, *Nucleosides Nucleotides*, 1997, **16**, 977–980.
70 M. T. Tierney and M. W. Grinstaff, *J. Org. Chem.*, 2000, **65**, 5355–5359.
71 B. Baumeister, N. Sakai and S. Matile, *Angew. Chem., Int. Ed.*, 2000, **39**, 1955–1958.
72 B. Baumeister, Thesis 3302, University of Geneva, 2001.
73 N. Sakai, N. Majumdar and S. Matile, *J. Am. Chem. Soc.*, 1999, **121**, 4294–4295.
74 B. Baumeister, A. Som, G. Das, N. Sakai, F. Vilbois, D. Gerard, S. P. Shahi and S. Matile, *Helv. Chim. Acta*, 2002, **85**, 2740–2753.
75 V. Borisenko, M. S. P. Sansom and G. A. Woolley, *Biophys. J.*, 2000, **78**, 1335–1348.
76 A. Som and S. Matile, *Chem. Biodiversity*, 2005, **2**, 717–729.
77 A. V. Hill, *Biochem. J.*, 1913, **7**, 471–480.
78 C. Park and R. T. Raines, *J. Am. Chem. Soc.*, 2001, **123**, 11472–11479.
79 J. Popot and D. Engelman, *Biochemistry*, 1990, **29**, 4031–4037.

80 N. Sakai, D. Houdebert and S. Matile, *Chem.–Eur. J.*, 2003, **9**, 223–232.
81 P. Talukdar, N. Sakai, N. Sordé, D. Gerard, V. M. F. Cardona and S. Matile, *Bioorg. Med. Chem.*, 2004, **12**, 1325–1336.
82 D. W. Deamer and D. Branton, *Acc. Chem. Res.*, 2002, **35**, 817–825.
83 N. Sordé, G. Das and S. Matile, *Proc. Natl. Acad. Sci. U. S. A.*, 2003, **100**, 11964–11969.
84 Y. Astier, O. Braha and H. Bayley, *J. Am. Chem. Soc.*, 2006, **128**, 1705–1710.
85 J. M. Lavin and K. D. Shimizu, *Org. Lett.*, 2006, **8**, 2389–2392.
86 O. H. Straus and A. Goldstein, *J. Gen. Physiol.*, 1943, **26**, 559–585.
87 S. Steenken and S. Jovanovic, *J. Am. Chem. Soc.*, 1997, **119**, 617–618.
88 S. L. Forman, J. C. Fettinger, S. Pieraccini, G. Gottarelli and J. T. Davis, *J. Am. Chem. Soc.*, 2000, **122**, 4060–4067.
89 N. V. Hud, P. Schultze, V. Sklenar and J. Feigon, *J. Mol. Biol.*, 1999, **285**, 233–243.
90 J. Shao and J. P. Tam, *J. Am. Chem. Soc.*, 1995, **117**, 3893–3899.
91 E. C. Rodriguez, K. A. Winans, D. S. King and C. R. Bertozzi, *J. Am. Chem. Soc.*, 1997, **119**, 9905–9906.
92 V. W. Cornish, K. M. Hahn and P. G. Schultz, *J. Am. Chem. Soc.*, 1996, **118**, 8150–8151.
93 P. T. Corbett, J. Leclaire, L. Vial, K. R. West, J.-L. Wietor, J. K. M. Sanders and S. Otto, *Chem. Rev.*, 2006, **106**, 3652–3711.
94 B. Levrand, Y. Ruff, J.-M. Lehn and A. Herrmann, *Chem. Commun.*, 2006, **41**, 2965–2967.
95 A. Som and S. Matile, *Eur. J. Org. Chem.*, 2002, 3874–3883.
96 P. M. Kramer, M.-P. Marco and B. D. Hammock, *J. Agric. Food Chem.*, 1994, **42**, 934–943.
97 H. D. King, D. Yurgaitis, D. Willner, R. A. Firestone, M. B. Yang, S. J. Lasch, K. E. Hellstrom and P. A. Trail, *Bioconjugate Chem.*, 1999, **10**, 279–288.
98 B. Abraham, S. McMasters, M. A. Mullan and L. A. Kelly, *J. Am. Chem. Soc.*, 2004, **126**, 4293–4300.

